Jointly published by
Akadémiai Kiadó, Budapest
and Kluwer Academic Publishers, Dordrecht

React.Kinet.Catal.Lett.
Vol. 75, No. 1, 3-12
(2002)

RKCL3916

SYNTHESIS OF LIGHT ALKENES ON MANGANESE PROMOTED IRON AND IRON-COBALT FISCHER-TROPSCH CATALYSTS

Sergio L. González-Cortés*, Serbia M. A. Rodulfo-Baechler, Alberto Oliveros[a], José Orozco*, Bernardo Fontal[b], Asiloé J. Mora[c] and Gerzon Delgado[c]

Laboratorio de Cinética y Catálisis, [b]Laboratorio de Organometálicos, [c]Laboratorio de Cristalografía Departamento de Química, Facultad de Ciencias, Universidad de Los Andes, Mérida 5101A-Venezuela

Received May 8, 2001
Accepted July 20, 2001

Abstract

The light alkenes formation capacity and the interaction of Mn with Fe and Fe-Co of Fischer-Tropsch catalysts have been studied. The samples were characterized by X-ray diffraction and temperature-programmed reduction. It was found that Fe-Co-Mn has a better catalytic stability than the Fe-Mn catalyst. It is proposed that iron particle size and its interaction with oxide and carbide phases produced during the catalytic reaction are mainly responsible for the high activity and light alkene selectivity.

Keywords: Fischer-Tropsch synthesis, alkenes, iron, cobalt, manganese

INTRODUCTION

The Fischer-Tropsch synthesis has great interest, due to the large variety of products that can be obtained, such as alkanes, alkenes and alcohols or narrow distributions of certain families (*i.e.* C_2-C_4 alkenes, gasoline, diesel) [1]. Therefore, selective formation of a narrow distribution of a certain family by this route, requires a deep molecular understanding of the surface chemistry of the hydrogenation reaction and subsequent polymerisation.

*Authors to whom correspondence should be addressed
[a]Present address: Laboratorio de Química Ecológica, Departamento de Química, Facultad de Ciencias, Universidad de Los Andes, Mérida 5101A-Venezuela

0133-1736/2002/US$ 12.00.

Fischer-Tropsch catalysts are mainly restricted to iron and cobalt and to a lesser extent to nickel. The combination of Fe-Mn [2-4], Co-Mn [5,6], and Fe-Co catalysts [7,8] with or without promoters favors the formation of C_2-C_4 alkenes. The first combination leads to mixed spinel phase formation in addition to the carbide phases [2,3], whereas the second consists mainly of MnO and small amounts of finely divided elemental cobalt [6]. On the other hand, Fe-Co catalyst favors an Fe-Co alloy formation [7,8]. The aim of this work is to combine the advantages of Fe-Mn and Co based Fischer-Tropsch catalysts to disperse metallic species on mixed spinel phases in order to inhibit metallic carbide formation and to study its influence on the catalytic and structural properties of Fe-Co-Mn Fischer-Tropsch catalyst.

EXPERIMENTAL

The α-Fe_2O_3 and MnO_2 were synthesized by the Kayo method [9] and by the precipitation method at constant pH [10], respectively. The precipitates were dried at 140°C for 16 h and calcined at 500°C for 5 h in dry air stream. CoO (98 %) was supplied by Merck. The Fe-Mn and Fe-Co-Mn catalysts with different formulations were prepared by mechanically mixing the precursory oxides, refluxing the aqueous mixtures at *ca.* 95°C for 3 h and partially drying by evaporation. The thick paste was then heated to dryness at 140ºC for 16 h and calcined at 500°C for 4 h in dry air stream. The catalyst (~8 g, >65 mesh) was placed on a fritted quartz disk and covered with quartz wool. Catalyst activation was done in situ with a hydrogen flow at 400°C for 24 h. Catalytic tests were carried out at 300°C and atmospheric pressure (0.1 MPa) with an inlet molar ratio (CO/H_2) of 1.0 and a gas-hour-space velocity (GHSV) of 300 h^{-1}. The reactor effluent gases were analyzed by gas chromatography with TCD and FID detection. CO conversion was determined from the difference between inlet and outlet CO amounts, while hydrocarbons selectivity was calculated by the relationship of all the products with carbon, excluding CO_2, and for alkene selectivity, methane was excluded as well. No significant amounts of condensed hydrocarbons and oxygenated compounds were detected. Semi-quantitative elemental proportions were verified by energy-dispersive X-rays spectroscopy (EDXS), using a Kevex model Delta-3 system connected to a Hitachi model S-2500 scanning electron microscope.

The crystalline phases characterization before and after reaction was made by X-ray diffraction (XRD) at room temperature using a Siemens D5005 diffractometer equipped with an X-ray tube (CuKα radiation: λ = 1.54059 Å; 40 kV, 30 mA), a diffracted beam graphite monochromator and fixed 1 mm aperture, 1 mm divergence, 0.1 mm monochromator and 0.6 mm detector slits. The specimens were prepared by grinding small quantitities of each sample in

an agate mortar and pestle and then loading into a flat sample holder, 25 mm in diameter and 2 mm deep. The X-ray powder diffraction patterns were collected at room temperature, in θ/θ reflection mode, scanning the specimens between 10°-100° 2θ, using steps of 0.02°, with counting time of 5s in each step. Quartz was used as an external standard. Temperature-programmed reduction (TPR) analysis was carried out on a Micromeritics TPD/TPR 2900 instrument. TPR profiles were done under the following conditions: reducing H_2-Ar mixture (10% H_2), 25 mL min^{-1} low rate, 5°C min^{-1} heating rate, and 10 to 20 mg sample weight.

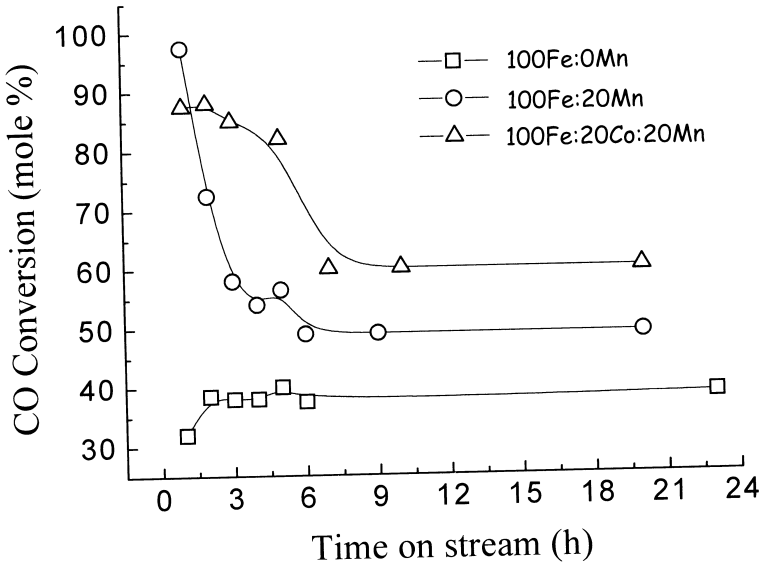

Fig. 1. Time-dependence of CO conversion of Mn-modified iron and iron-cobalt Fischer-Tropsch catalysts at 300°C, 0.1 MPa, GHSV of 300 h^{-1}, and H_2/CO of 1

RESULTS AND DISCUSSION

Carbon monoxide conversion as a function of time on stream for metallic iron, 100Fe:20Mn, and 100Fe:20Co:20Mn catalysts is shown in Fig. 1. Steady state was reached after 6-7 h of reaction for 100Fe:20Mn and 100Fe:20Co:20Mn catalysts, whereas it was reached after 3 h for bulk iron. During the time on stream the Fe-Mn and Fe-Co-Mn catalysts displayed

deactivation, especially the Mn-modified iron catalysts whose activity is reduced in half; the unpromoted iron catalyst showed some activation early in the reaction. As the CO conversion changes significantly with manganese and cobalt addition, this shows clearly that the metallic iron catalyst activity can be effectively modified by the addition of these promoters.

Table 1 shows CO conversion and product distribution for Mn-modified iron catalyst under steady state conditions. These systems show lower CO conversion than unpromoted iron, except the 100Fe:20Mn system. CO_2 selectivity decreases steadily as the Mn loading is increased, whereas hydrocarbon selectivity is increased by 20%. On the other hand, methane selectivity is highest for the 100Fe:20Mn catalyst and decreases at higher and lower Mn compositions. Alkenes selectivity and alkene/alkane relationship (O/P) reaches a maximum (1.8) for the 100Fe:20Mn catalyst. This is probably due to Fe^{3+} oxide phase formation, which has a low surface area and porosity that inhibit the secondary reactions of alkenes [11]. At approximately isoconversion of CO the alkene/alkane ratio for 100Fe:50Mn increases about 70% compared with the 100Fe:5Mn catalyst. It shows clearly that alkene selectivity can be modified by manganese addition.

Table 1

CO conversion and products distribution of Mn-modified iron catalyst at 300°C, 0.1 MPa, GHSV of 300 h^{-1}, and inlet H_2/CO of 1

	Molar proportion (Fe:Mn)				
	100:0	100:5	100:20	100:50	100:100
XCO (mole %)	38.0	26.5	49.0	20.0	10.0
SCO_2 (mole %)	71.4	72.7	66.5	62.0	52.2
SHC	28.6	27.3	33.5	38.0	47.8
HC (mole %)					
CH_4	37.7	46.0	65.4	48.9	43.8
C_2	5.6	19.8	7.7	11.8	2.0
$C_2^=$	18.0	10.5	10.8	9.4	15.8
C_3	17.8	4.0	1.3	2.9	7.3
$C_3^=$	7.7	4.6	6.1	12.0	4.9
C_4	4.0	3.7	1.2	1.4	4.9
$C_4^=$	6.0	4.4	1.5	2.0	5.5
C_5	2.0	4.0	2.0	7.0	8.0
$C_5^=$	1.2	3.0	4.0	4.6	7.8
$S(C_2\text{-}C_5)^=$	52.8	41.6	64.7	54.8	60.5
O/P[a]	1.1	0.7	1.8	1.2	1.5

[a]Alkene/Alkane ratio

The Fe:Co catalyst was prepared with a Co molar proportion of 20, within the concentration range generally used in Fischer-Tropsch synthesis [12]. CO conversion and product distribution of the Mn-modified 100Fe:20Co catalyst is presented in Table 2. Under the reaction conditions used, a Co molar proportion of 20 addition on iron decreases the activity and selectivity to hydrocarbons, with the corresponding increase in CO_2 selectivity compared with the metallic iron catalyst, probably due to an oxidized phase participation during the catalytic cycle. The strong hydrogenation activity of cobalt [13]

Table 2

CO conversion and product distribution of Mn-modified 100Fe:20Co catalyst at 300°C, 0.1 MPa, GHSV of 300 h^{-1}, and inlet H_2/CO of 1

	Molar proportion (Fe:Co:Mn)				
	100:20:0	100:20:10	100:20:20	100:20:50	100:20:100
XCO (mole %)	26.0	53.1	60.0	36.0	25.4
SCO_2 (mole %)	95.7	71.0	46.8	73.9	63.2
SHC	4.3	29.0	53.2	26.1	36.8
HC (mole %)					
CH_4	54.0	85.4	34.0	76.7	81.8
C_2	10.0	4.9	12.0	7.6	4.5
$C_2^=$	2.2	4.1	12.0	2.8	2.8
C_3	7.5	2.1	3.2	0.8	2.3
$C_3^=$	4.0	1.7	9.0	1.2	1.9
C_4	5.0	0.4	3.0	4.7	0.3
$C_4^=$	6.0	0.4	4.0	1.2	0.3
C_5	4.0	0.7	11.0	1.0	4.0
$C_5^=$	7.3	0.3	11.8	4.0	2.1
$S(C_2\text{-}C_5)^=$	42.4	44.5	55.8	39.5	39.0
O/P[a]	0.7	0.8	1.3	0.7	0.6

[a]Alkene/Alkane ratio

entails a higher methane selectivity and smaller alkene/alkane relationship. Mn addition to the 100Fe:20Co catalyst was found to improve CO conversion as the Mn molar proportion increases. Hydrocarbons selectivity is highest for the 100Fe:20Co:20Mn catalyst and decreases at higher and lower Mn compositions, whereas CO_2 selectivity shows a minimum at that composition. Methane selectivity shows a minimum for the 100Fe:20Co:20Mn catalyst without a clear tendency in all the Mn composition range studied. This catalyst presented a high selectivity to C_2 and C_5 products as well. Alkene selectivity and alkene/alkane relationship (O/P, 1.3) are highest for the 100Fe:20Co:20Mn catalyst and

decrease at higher and lower Mn compositions. Considering that both alkene selectivity and the O/P relationship were smaller for the Fe-Co-Mn catalysts compared with the Fe-Mn catalysts, suggests that cobalt has an important participation in secondary hydrogenation reactions and that an Fe-Co alloy which favors alkene selectivity [7,8] is not being formed. The Fe:Mn molar relationship of 5 provides the optimum Mn promoter effect on the particles of metallic iron producing high CO conversion, high alkene selectivity and a high alkene/alkane relationship.

The Mn influence on the structure and reducibility of the α-Fe_2O_3 and Fe-Co catalysts, is detailed for four Mn compositions that indicates the general tendency of the systems studied.

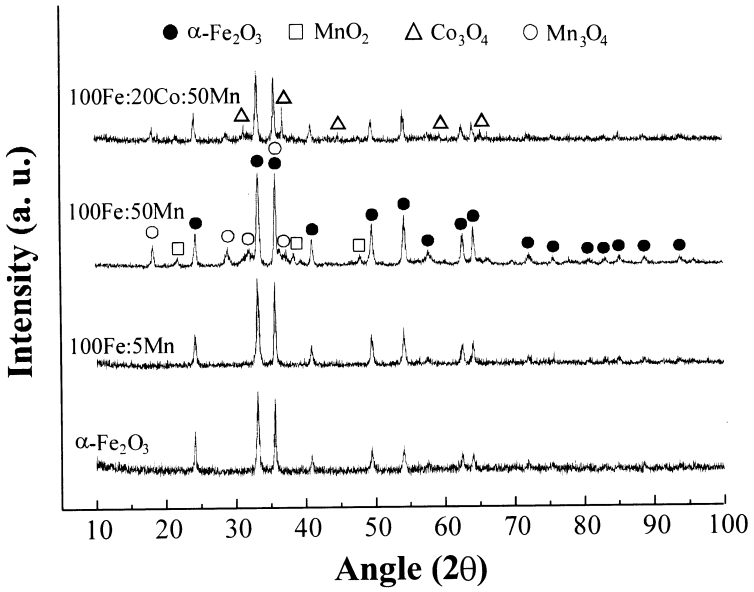

Fig. 2. X-ray diffraction powder patterns of fresh Mn-modified iron and iron-cobalt Fischer-Tropsch catalysts

The X-ray powder diffraction patterns of fresh Mn-modified iron and iron-cobalt Fischer–Tropsch catalysts are shown in Fig. 2. Crystalline phases identification in the samples studied was carried out using the diffractometer

analytical software after a meticulous revision of the PDF-ICDD database of crystalline materials [14]. Only hematite (α-Fe_2O_3) was identified in the pure iron catalyst. The diffraction pattern for the 100Fe:5Mn formulation does not significantly change from hematite, which suggests the incorporation of manganese into the hematite structure to form α-$(Fe_{1-x}Mn_x)_2O_3$, as has been reported in the literature [3]. The 100Fe:50Mn catalyst shows the hematite diffraction pattern as the main crystalline phase, and some diffraction lines associated with Mn_3O_4 and MnO_2 phases. The diffraction pattern for the 100Fe:20Co:50Mn catalyst corresponds to Co_3O_4 spinel, hematite and Mn_3O_4 spinel phases. $Co_xFe_{3-x}O_4$ and $Co_xMn_{3-x}O_4$ mixed-metal oxides formation is not detected, probably due to the synthesis method used (mechanical mixtures of the precursor metal oxides). The findings clearly indicate that cobalt addition and the addition of different manganese amounts produce a number of oxide phases as precursors of active sites in the Fischer-Tropsch synthesis.

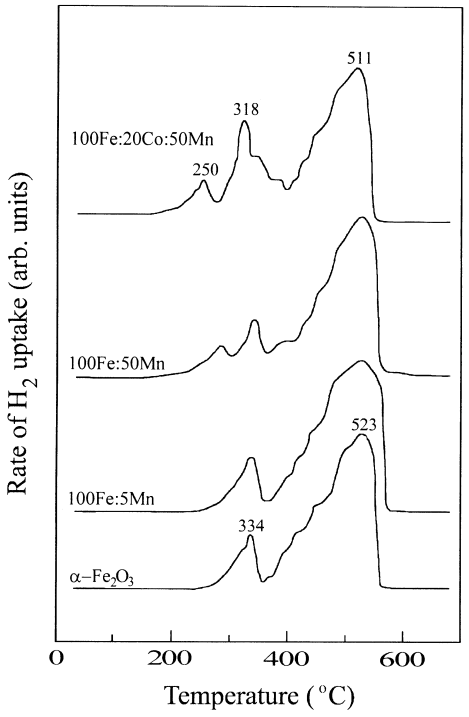

Fig. 3. Temperature-programmed reduction profiles of Mn-modified iron and iron-cobalt Fischer-Tropsch catalysts

Temperature-programmed reduction profiles of Mn-modified iron and iron-cobalt Fischer–Tropsch catalysts are displayed in Fig. 3. Hematite (α-Fe_2O_3) shows two hydrogen consumption peaks, a smaller one at 334°C corresponding to Fe_2O_3 to Fe_3O_4 reduction and a larger asymmetric peak at higher temperature (523°C) due to Fe^{3+} reduction to Fe^{2+} and then to metallic iron [15]. The clear separation between these two reduction steps may be due to water present in the reaction mixture [16]. The reduction profile for the 100Fe:5Mn catalysts is similar to α-Fe_2O_3, whereas the 100Fe:50Mn catalyst show a new small peak at lower temperature (285°C) due to a reducibility increase by Mn incorporation in the iron oxide structure to form α-$(Fe_{1-x}Mn_x)_2O_3$, as suggested by XRD. **C**obalt addition produces both an increase of an intermediate peak at 318°C due to cobalt oxide (Co_3O_4) and a reducibility increase for the catalyst (reduction peak maximum at 511°C); this explains the catalyst hydrogenation activity for this composition, reducing the O/P relationship and favoring methane formation compared with the Fe-Mn catalyst (see Tables 1 and 2).

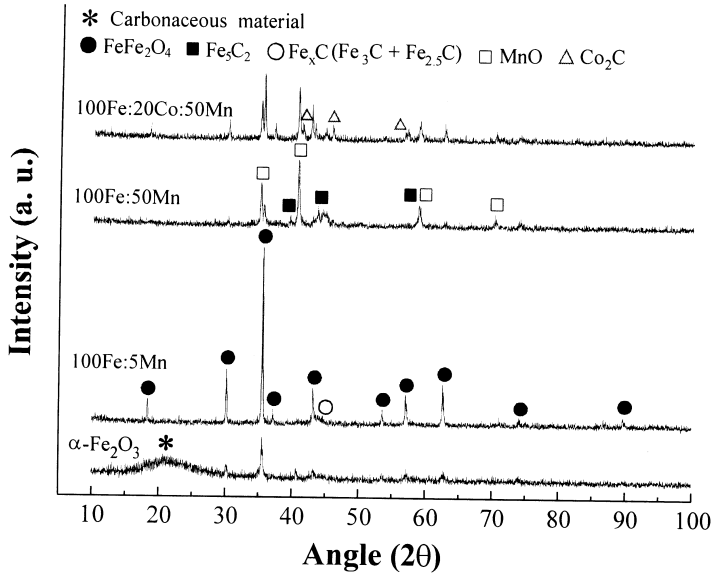

Fig. 4. X-ray diffraction powder patterns of used Mn-modified iron and iron-cobalt Fischer-Tropsch catalysts

The X-ray powder diffraction patterns for used Mn-modified iron and iron-cobalt Fischer–Tropsch catalysts are shown in Fig. 4. The pure iron catalyst shows magnetite (Fe_3O_4) as the majority phase in addition to Fe_xC iron-carbide phases formed by a $Fe_{2.5}C$ and Fe_3C mixture and an amorphous carbonaceous deposit, which does not seem to affect catalytic stability. The 100Fe:5Mn formulation displays a mixed spinel phase $(Fe_{1-x}Mn_x)_3O_4$ as the main crystalline phase, and weak peaks corresponding to Fe_xC iron-carbide phases. Carbonaceous species formation is suppressed, probably due to high iron dispersion on the mixed-metal oxide surface, preventing coalescence of iron centers into large particles. However, the CO conversion for the 100Fe:5Mn catalyst in the steady state is lower than for the iron catalyst (See Table 1). This could be due to metallic iron oxidation to mixed-metal oxide during the first hours on stream due to an oxidizing reaction atmosphere produced by high initial CO conversion (~60-45 %) [2]. The diffraction pattern for the 100Fe:50Mn catalyst shows manganese oxide (MnO) and Hägg carbide (χ-Fe_5C_2) as the main crystalline phases, whereas the mixed spinel phase is drastically reduced. However, CO conversion for this formulation is lower than for the iron catalyst (See Table 1). This may be attributed to carbide formation and elemental iron sintering effects during the first hours of catalytic activity. The X-ray powder diffraction pattern for the 100Fe:20Co:50Mn catalyst shows both MnO and carbide phases, in addition to a clear mixed-metal oxide enrichment compared with the 100Fe:50Mn catalyst; this is reflected on a higher activity (See Tables 1, 2). Based on these findings, the differences in steady state activity can be ascribed to an appropriate proportion of catalyst components that favors mixed spinel phase and MnO formation in adequate amounts to inhibit oxidation, carburization, and sintering effects of the metallic iron particles.

It is well known that during Fischer-Tropsch synthesis on iron-based catalysts carbide phases are produced [1,12]. The Fe-Mn catalyst with small Mn amounts shows small $Fe_{2.5}C$ and Fe_3C mixtures, whereas Mn-rich catalysts display a clear Hägg carbide enrichment (See Fig. 4), due to a larger fraction of large iron particles [3]. Both the iron carbides and the mixed spinel phase composition decrease significantly on the Fe-Co-Mn catalyst and a higher catalytic stability is attained compared with the Fe-Mn catalyst.

Product distribution obtained with the Fe-Mn and Fe-Co-Mn catalysts indicate that the former presents a slight descent and the latter displays a minimum for CO_2 selectivity as the Mn loading is changed (See Tables 1 and 2). This is likely due to a mixed spinel phase decrease since magnetite has been proposed as the most active phase for the water-gas shift reaction on iron catalysts [1]. Methane selectivity reaches a maximum for the 100Fe:20Mn composition and a minimum for the 100Fe:20Co:20Mn catalyst, probably due to changes in surface mobility of methanation sites [1]. Alkene selectivity and

the O/P relationship show a maximum for the catalysts with a molar relationship of 5 (Fe/Mn) (See Tables 1 and 2), whereas the alkene/CH_4 relationship for the 100Fe:20Co:20Mn catalyst (1.08) is higher than for the 100Fe:20Mn catalyst (0.34). This is attributed to a higher stability of metallic iron on a mixed spinel phase [2] that decreases the methanation sites.

Even though the catalyst preparation method and the reaction conditions used in this study are different to those used by other investigators, the molar relationship of 5 (Fe/Mn) coincides with an activity maximum and alkene selectivity reported by Das *et al.* [4], and a maximum alkene selectivity reported by Malesa and Baerns [2]. This suggests that competition among the oxidation, reduction, sintering, and carburization processes during synthesis occur under optimal conditions, most likely due to a conjugated effect of the iron particle size and their interaction with the oxide and carbide phases produced during the catalytic reaction.

Acknowledgments. The authors are deeply grateful to CDCHT-ULA and CONICIT (Grant LAB-97000821) for their financial support.

REFERENCES

1. G.P. Van der Laan, A.A.C.M. Beenackers: *Catal. Rev.-Sci. Eng.*, **41**, 255 (1999).
2. R. Malesa, M. Baerns: *Ind. Eng. Chem. Res.*, **27**, 279 (1988).
3. J.B. Butt: *Catal Lett.*, **7**, 83 (1990).
4. C.K. Das, N.S. Das, D.P. Choudhury, G. Ravichandran, D.K Chakrabarty: *Appl. Catal. A,* **111**, 119 (1994).
5. S. Colley, R.G. Coppertwaite, G.J. Hutchings, M. Van der Riet: *Ind. Eng. Chem. Res.*, **27,** 1339 (1988).
6. M.J. Keyser, R.C. Everson, R.L. Espinoza: *Appl. Catal. A,* **171**, 99 (1998).
7. C. Cabet, A.C. Roger, A. Kiennemann, S. Lakamp, G. Pourroy: *J. Catal.*, **173**, 64 (1998).
8. F. Tihay, A.C. Roger, A. Kiennemann, G. Pourroy: *Catal. Today*, **58**, 263 (2000).
9. A. Kayo, T. Yamaguchi, K. Tanabe: *J. Catal.*, **83**, 99 (1983).
10. W-D. Deckwer, Y. Serpemen, M. Ralek, B. Schmidt: *Ind. Eng. Chem. Process Des. Dev.*, **21**, 222 (1982).
11. H.J. Krebs, H.P. Bonzel, W. Schwarting, G. Gafner: *J. Catal.*, **72**, 199 (1981).
12. J.P. Hindermann, G.J. Hutchings, A. Kiennemann: *Catal. Rev.- Sci. Eng.*, **35,** 1 (1993).
13. R.B. Anderson: *The Fischer Tropsch Synthesis*, p. 129. Academic Press, New York 1984.
14. *Powder Diffraction File* (PDF-2, Set 1-49), International Centre for Diffraction Data, 12 Campus Boulevard, Newtown Square, PA, USA (1999).
15. P.A. Webb, C. Orr: *Analytical Methods in Fine Particle Technology*, p. 265. Micromeritics Instrument Corporation, Norcross, GA, USA (1997).
16. O.J. Wimmers, P. Arnoldy, J.A. Moulijn: *J. Phys. Chem.*, **90**, 1331 (1986).